coatings

MDPI

Article

Study of Calcium Ethoxide as a New Product for Conservation of Historical Limestone

Martina Zuena [1,2,*], Patrizia Tomasin [3], Dória Costa [4], José Delgado-Rodrigues [4] and Elisabetta Zendri [2]

1 Department of Molecular Science and Nanosystem, Ca' Foscari University of Venice, 30170 Venezia Mestre, Italy
2 Department of Environmental Sciences, Informatics and Statistics, Ca' Foscari University of Venice, Via Torino 155, 30170 Venezia Mestre, Italy; elizen@unive.it
3 ICMATE, Istituto di Chimica della Materia Condensata e di Tecnologie per l'Energia, CNR, Area della Ricerca di Padova, Corso Stati Uniti 4, 35127 Padova, Italy; patrizia.tomasin@cnr.it
4 National Laboratory of Civil Engineering, Avenida do Brasil, 101, 1700-066 Lisbon, Portugal; drcosta@lnec.pt (D.C.); delgado@lnec.pt (J.D.-R.)
* Correspondence: martinazuena@gmail.com; Tel.: +39-3476418021

Received: 20 February 2018; Accepted: 12 March 2018; Published: 13 March 2018

Abstract: The combination of multiple physical, chemical and biological factors causes the weathering of limestone used in the field of cultural heritage. To overcome the limitations of traditional consolidating products and to meet the requirements of the historical building substrates, during the European collaborative project NANOMATCH, alkaline earth alkoxides were developed and studied as consolidating agents for limestone. Among these new products, calcium ethoxide, with the formula $Ca(OEt)_2$, was chosen for this study and investigated in depth as an alternative consolidating treatment. It was first characterized through a study of the carbonation process: its kinetics, reaction pathway and the evaluation of formed mineralogical phases. Subsequently, it was applied on limestones with different total open porosity to test its performance as a consolidating agent. The compatibility and the efficiency of the treatment were investigated with a multi-technique approach and compared with results obtained with a reference product, based on nanolime. This study indicates that calcium ethoxide shows better results with respect to the reference product, both in terms of compatibility and consolidation effect.

Keywords: calcium ethoxide; calcium alkoxide; calcium carbonate polymorphs; consolidation treatment; limestone; consolidation effectiveness; colorimetry; microdrilling; ultrasonic velocity

1. Introduction

The constant exposure of limestone to several weathering factors (e.g., atmospheric pollution [1,2], freeze-thaw cycles [3], salt crystallization [4] and biological colonization [5]), combined with their compositional and textural characteristics causes an increase in porosity and a loss of material cohesion. Today, the knowledge acquired about the deterioration processes has promoted the improvement of stone cohesion and adhesion and the preservation of buildings and decorative surfaces of architectural monuments through consolidation interventions. However, the consolidation of limestone is still an open debate.

Therefore, during the EU-Project NANOMATCH (nano-systems for the conservation of immoveable and moveable polymaterial cultural heritage in a changing environment FP7/2007-2013, Grant Agreement No. 283182), new conservation products, calcium alkoxides, were developed and studied. They are innovative conservation products to consolidate carbonate stones and wall paintings.

In fact, these compounds, dissolved in a proper organic solvent, penetrate inside the stone and react with humidity and atmospheric carbon dioxide to form calcium carbonate. Through this carbonation process, the starting alcohol evaporates and is released. This behavior makes them suitable for consolidation of carbonate supports, such as wall paintings, plasters and building stone materials [6–10].

Previous studies [6,11,12] showed that the carbonation process of calcium alkoxides can follow two different pathways. The first is an insertion of a CO_2 molecule within the Ca–O bond with the formation of an intermediate alkyl carbonate followed by hydrolysis and alcohol elimination. The second is a reaction involving first hydrolysis of the alkoxide with the formation of calcium hydroxide as the intermediate, which subsequently carbonates.

In this study, the performance of calcium ethoxide, a nanosuspension produced by ABCR labs during the European Project, as stone consolidant for carbonate stones was investigated and compared with a reference product based on nanolime, CaLoSil E50. During the carbonation process of this nanolime, atmospheric CO_2 reacts with calcium hydroxide, leading to the precipitation of calcium carbonate. The work began with a first characterization of the product: the study of the kinetic and reaction pathway of the carbonation process, as well as the evaluation of mineralogical phases formed from the reaction of this product with air. Subsequently, the product was applied on mock-ups of three limestones characterized by a different type of porosity and widely used in the field of cultural heritage, in Italy. Several types of analyses and techniques were used, before and after the application of the product, to understand its performance as a consolidating treatment.

2. Materials and Methods

The product calcium ethoxide, labelled in the text as ET was developed by ABCR labs (Spain). It is a nanosuspension of $Ca(OEt)_2$ in a 1:3 mixture (v/v %) of ethanol and tetrahydrofuran with an initial calcium concentration of 46.5 g/L and average particles' dimension of 295 nm (determined by DLS analysis, Malvern Panalytical Ltd., Nottingham, UK). Based on previous studies carried out during the NANOMATCH project, a calcium concentration of 20 g/L showed the best results, as it combined a good consolidation effect without causing an unacceptable color change of the surface [13]. Therefore, the initial nanosuspension was diluted in ethanol to reach a calcium concentration of 20 g/L.

CaLoSil E50® (Salt Lake City, UT, USA) labelled in the text as CA, was used as a reference product. It is produced by IBZ-Salzchemie (GmbH & Co. KG, Teningen, Germany), and according to the technical sheet, it is composed of stable colloidal $Ca(OH)_2$ nanoparticles (50–250 nm) dispersed in ethanol [14]. In this case, the calcium concentration was 27.05 g/L; therefore, to achieve a calcium concentration of 20 g/L, the same chosen for calcium ethoxide, it was diluted with ethanol.

Fourier transform infrared spectroscopy (FT-IR) measurements were performed to study the kinetic and the reaction pathway of the carbonation process of $Ca(OEt)_2$, both alone and mixed with the powdered stones. This was to understand if the presence of the substrate could affect the carbonation process and to evaluate the mineralogical phases of $Ca(OEt)_2$ and CaLoSilE50 coating on a glass slide, kept at different relative humidities. A Nicolet microscope connected to a Nicolet 560 FT-IR system, equipped with an MCT (mercury-cadmium-telluride) detector working in reflectance mode was used. The spectra were collected within a range of 4000–650 cm^{-1}, with a resolution of 4 cm^{-1}, and 64 scans were collected each time. The analyzed area consists of a square of 50 × 50 μm^2. For the kinetic measurements, a small drop of calcium ethoxide was laid down on a glass surface, and μFT-IR spectra were acquired at different times, from the beginning of the analysis till complete conversion of compounds to calcium carbonate. The analyzed samples were kept at laboratory humidity and temperature conditions during the period of analysis. Moreover, the mineralogical phases were determined by analyzing the products previously deposited on a glass surface, left to dry and properly maintained at different relative humidities (RH), 50% and 90%, to simulate a drier and a very humid environment, respectively. The samples were kept in two different dryers maintained in a room at controlled temperature (20–22 °C). The different relative humidity conditions in the

two dryers were obtained by inserting a beaker with a saturated solution of a specific salt [15]; saturated solutions of calcium nitrate and potassium nitrate were prepared to create a 50% RH and a 90% RH environment, respectively. Relative humidity conditions were monitored with a relative humidity sensor (Oregon Scientific™ Wireless Weather Station BAR388HG). To perform μFT-IR analysis of the resulting coatings, a small quantity of product was taken away from the deposit and rolled out on a glass surface. It was analyzed at two weeks, one month and three months of exposure X-ray diffraction (XRD), performed with a Philips X'Pert PW3710 diffractometer (Philips Gloeilampenfabrieken N.v., Eindhoven, The Netherlands) with a Bragg–Brentano geometry and an incident radiation of Cu kα (40 kV and 30 mA), was used to complete the study of the mineralogical phases of the products' coating stored at different RH conditions. All the measurements were carried out in continuous mode in the range $10° < 2\theta < 70°$, with a step size of 0.02° and an acquisition time of 4 s. Also in this case, the analysis was carried out at two weeks, one month and three months.

Three limestones widely used in the field of Italian cultural heritage both as building materials and for works of art were selected on the basis of different types and values of total open porosity. Noto stone, Vicenza stone and Lecce stone were chosen. Noto stone, extracted in a quarry near the city of Noto, has an open porosity of 30% and pores size between 1 and 4 μm. The porosity of Vicenza stone is 31% with a bimodal pore size between 0.1–0.4 and 1–11 μm. It is classified as a calcarenite, and it was extracted from Badia quarry, near the city of Vicenza. Lecce stone with a porosity of 34% and pore size between 0.1 and 2 μm presents fragments of fossils and microfossils of marine organisms together with other minerals such as quartz, various feldspars, glauconite and phosphates, and it was extracted from quarries near the city of Lecce.

$Ca(OEt)_2$ and CaLoSil E50 were applied on stone materials with two different application procedures: by brush till saturation (B1) and by brush with a pre-set number of brush strokes (B2) Brush till saturation was chosen because it is usually performed in situ; while brushing with a pre-set number of brush strokes was carried out to understand the compatibility between the product and the stone supports. In the case of application B1, treatments were applied till saturation of the surface was reached, intended as the condition when stone surface remains wet for 1 min. In the case of application B2, the number of applications was calculated in order to avoid a color change of the treated surface. A colorimetric measurement was performed after each brush stroke of $Ca(OEt)_2$ till the maximum value of $\Delta E^* < 5$ was reached. To better compare the results obtained with the reference product and to limit the number of variables, CaLoSil E50 was applied using the same number of brush strokes.

For each type of application and treatment, the amount of retained product, evaluated by weighing samples before and at one month from treatment application, is expressed as the weight of product per unit surface (kg/m^2) and reported as the range of the value between the minimum and the maximum quantities.

To work on weathered materials, the lithotypes were submitted to an artificial ageing based on thermal cycles, six daily heating-cooling cycles: 100 °C for 6 h, cooling to room temperature for 6 h, chilling to −20 °C for 6 h and finally warming to room temperature for 6 h [16]. All the following tests were performed on aged samples.

Changes in total open porosity due to the ageing process and to the application of products was calculated on dried samples by mercury intrusion porosimetry (MIP) according to the NORMAL 4/80 [17]. Pascal 140 and Pascal 240 Thermo Nicolet instruments (CE Elantech, Inc., Lakewood, NJ, USA) were used for the individuation of macropores and mesopores, respectively.

Water absorption through capillarity was carried out according to the procedure described in the normative UNI EN 10859:2000 [18]. Three samples ($3 \times 3 \times 3$ cm^3) for each type of stone were covered with aluminum tape leaving only one surface free, the one on which the consolidating treatments were applied. After the application of the products, the surface put in contact with the water was the treated one. The capillary water absorption coefficient (CWAC) corresponds to the angular coefficient of the initial stage of the capillary absorption curve.

Water vapor permeability, expressed as the water vapor permeability coefficient (g), was carried out according to the standard DIN 52 615 [19]. Three samples ($5 \times 5 \times 1$ cm^3) for each type of stone were covered on the lateral surfaces and fixed on open vessels half-filled with a saturated salt solution of potassium nitrate to reach an internal relative humidity of 93%. These vessel-sample systems were allocated in a room with constant air temperature (23 °C) and relative humidity (50%), and they were weighed at specific time intervals till reaching a steady state condition.

Color measurements, performed to evaluate the aesthetic compatibility of $Ca(OEt)_2$ and CaLoSil E50 with the stone supports, were made in the CIE*L*a*b** color space. The total color difference $\Delta E^*$was computed as reported in Equation (1):

$$\Delta E^* = \sqrt{\Delta L^{*2} + \Delta a^{*2} + \Delta b^{*2}} \quad (1)$$

According to the NORMAL 43/93 [20], color data were acquired with a CM2600d Konica Minolta portable spectrophotometer with a D65 illuminant and 10° standard observer. The instrument has a 5-mm diameter measurement area, and it is set to quantify the potential specular component included (SCI). These data were acquired from prismatic samples of $5 \times 10 \times 2$ cm^3, before and after treatment.

Scanning electron microscopy (SEM) images were obtained to observe the morphology changes induced by the applied products on the treated surface. These analyses were performed on small fragments of samples using an FEI Quanta 200 FEG-ESEM (FEI Czech Republic s.r.o, Brno, Czech Republic). The observations were carried out in high vacuum conditions, after metallization with carbon, with an ETD (Everhart Thornley Detector) detector and at low vacuum conditions with an LFD (Large Field Detector) detector. Different magnifications were used according to the information to be acquired.

Ultrasonic pulse velocity (UPV) and the Drilling Resistance Measurement System (DRMS) were used on the same dried samples ($5 \times 5 \times 5$ cm^3) and only for specimens treated with application B1. UPV was performed with the direct transmission method by using a pulse generator (G. Steinkamp BP-7, Laboratory for Applied Physics, Bremen, Germany) coupled to 45-kHz transducers. The ultrasonic transmitter and receiver were placed opposite each other, and the measurements were done in profile proceeding from the treated surface to the bottom. The results are expressed as the mean value of three measurements at each point, established with a 5–mm interval, from 5–45 mm.

The Drilling Resistance Measurement System (DRMS, Sint Technology, s.r.l., Calenzano, Italy) was used with a 5 mm-diameter flat diamond drill bit. The operating conditions were the following: advancing rate of 10 mm/min, rotational speed of 300 rpm and target penetration depth of 10–15 mm, in accordance with the type of limestone. Data for treated and untreated conditions were obtained from the same mock-ups, on opposing surfaces.

3. Results and Discussion

3.1. Kinetic and Reaction Pathway

Figure 1a reports μFT-IR spectra collected at different times and, therefore, the evolution of calcium carbonate formation from the beginning of the reaction until two weeks later. After alcohol evaporation in the first instants, a broad vibrational band related to the presence of carbonate ion in the region between 1400 and 1480 cm^{-1} (asymmetric stretching mode υ_3 of carbonate ion) starts to be present after two minutes from the beginning of the reaction (Figure 1b) [21–23]. After six hours (Figure 1c), only peaks related to amorphous calcium carbonate (ACC) are present: 1406–1480 cm^{-1} (asymmetric stretching mode υ_3 of the carbonate ion), 1060 cm^{-1} (symmetric stretching mode υ_1 of the carbonate ion) and 864 cm^{-1} (out of plane bending mode υ_2 of the carbonate ion) [24–26]. Furthermore, the broad band between 2700 and 3600 cm^{-1} related to O–H stretching is present from the beginning until two weeks later and corresponds to structural water within ACC [27,28]. After two weeks (green spectrum in Figure 1a), the results remain constant, showing the presence of ACC, confirmed by the absorption peak at 864 cm^{-1}.

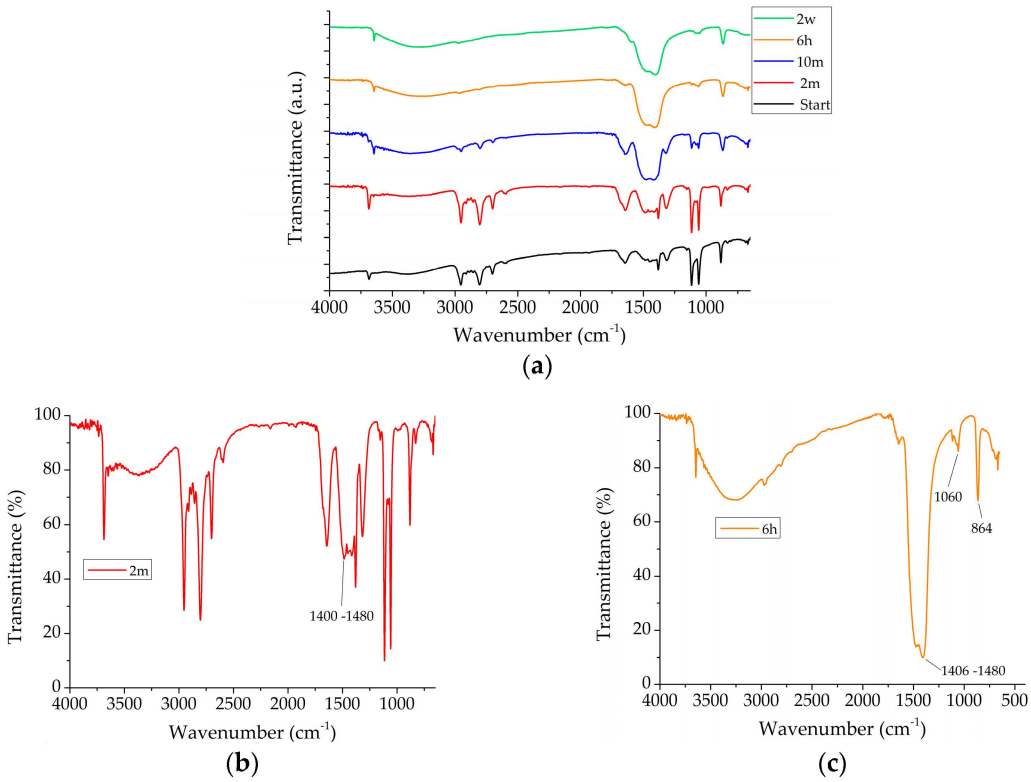

Figure 1. μFT-IR spectra showing kinetic process of $Ca(OEt)_2$: (**a**) entire process; (**b**) spectrum acquired after two minutes; (**c**) spectrum acquired after six hours. Time intervals: start, beginning of the reaction; 2 m, two minutes; 10 m, ten minutes; 6 h, six hours; 2 w, two weeks.

Regarding the reaction pathway, absorption peaks at 1650 cm^{-1} and 1320 cm^{-1}, corresponding respectively to asymmetrical and symmetrical stretching of $CH_3CH_2OCO_2$, have been observed (Figure 2) [6,29]. These peaks are related to the insertion of CO_2 in the Ca–O bond of calcium ethoxide producing the corresponding calcium ethyl carbonate, which successively transforms into $CaCO_3$ by hydrolysis. In fact, this absorption peak decreases until it disappears in about six hours, being replaced by the characteristic signals of amorphous $CaCO_3$. However, the presence of an absorption peak at 3645 cm^{-1} related to O–H stretching [28,30] suggests also a second kinetic pathway due to a hydrolysis process leading first to the formation of $Ca(OH)_2$, which successively undergoes a carbonation process through CO_2 insertion into the Ca–O bond of $Ca(OH)_2$. Small signals at 1470–1483 cm^{-1} and 1380–1410 cm^{-1} evidence the formation of various coordinated bicarbonate groups, as reported in [6,7], which overlap $CaCO_3$ absorption bands.

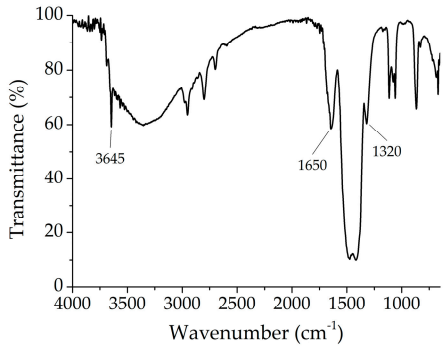

Figure 2. μFT-IR spectrum showing the reaction pathway of $Ca(OEt)_2$.

The peak related to O–H stretching (3645 cm^{-1}) is still present after two weeks, as shown in the green spectrum in Figure 1a, and it highlights that the carbonation process is not concluded.

The presence of powdered limestones mixed with the analyzed product did not affect the kinetic and reaction pathway of $Ca(OEt)_2$.

3.2. Coating Investigation

Results obtained after two weeks by keeping $Ca(OEt)_2$ at 50% RH and 90% RH, for both XRD and μFT-IR analyses, are reported in Figures 3 and 4, respectively. At 50% RH, XRD results show the presence of portlandite with a hexagonal structure and the main characteristic reflections at 2θ = 17.9°/34° (ICCD: 00-001-1079) together with a carbonatic phase also characterized by vaterite with a hexagonal structure and main reflection at 2θ = 27° (ICCD: 00-001-1033) [31–34] (Figure 3a). The μFT-IR spectrum confirms the presence of vaterite with a characteristic absorption peak at 1088 cm^{-1} [26] and portlandite with an absorption peak at 3645 cm^{-1} due to O–H stretching (Figure 3b).

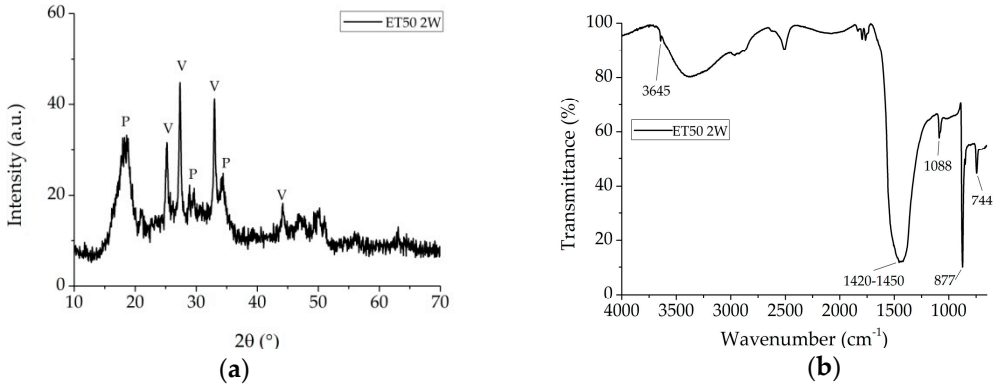

Figure 3. $Ca(OEt)_2$ at 50% RH after two weeks (ET50 2W): (**a**) XRD pattern; (**b**) μFT-IR spectrum. XRD peak assignments: P, portlandite; V, vaterite.

At 90% RH (Figure 4a), there is still portlandite with the same structure and the co-presence of carbonatic phases of vaterite and calcite. The latter has a rhombohedral structure and principal reflection at 2θ = 29° (ICCD: 01-072-1651) [35].

μFT-IR results are consistent with XRD; in fact, at 90% RH, vaterite, calcite (713 cm^{-1}) and portlandite can be ascertained from the spectrum (Figure 4b). The presence of portlandite after two weeks proves that the carbonation process is not concluded, confirming the kinetic measurements. However, differently from this, the final calcium carbonate is present in a crystalline phase. This difference is probably due to the RH condition, which remains constant during all of the analyzed period.

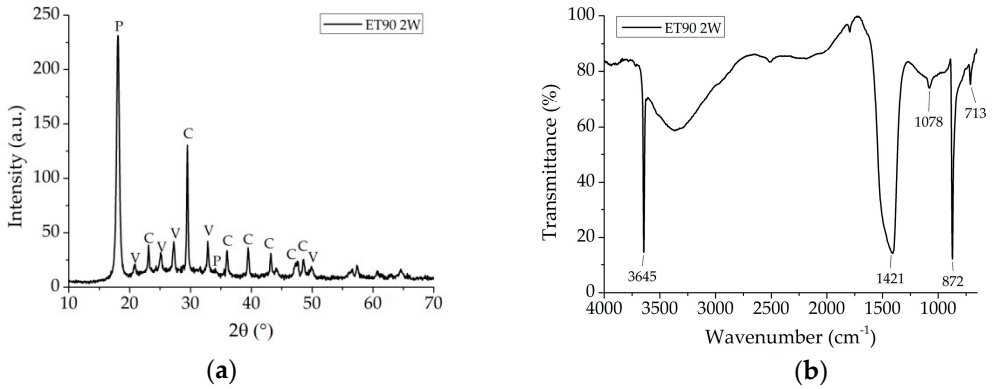

Figure 4. $Ca(OEt)_2$ at 90% RH after two weeks (ET90 2W): (**a**) XRD pattern; (**b**) μFT-IR spectrum. XRD peak assignments: P, portlandite; C, calcite; V, vaterite.

XRD and μFT-IR measurements after one month at 50% RH show only the presence of vaterite, while peaks related to portlandite disappear, indicating that the carbonation process is ended. At 90% RH, both the presence of vaterite (ICCD 00-033-0268) and of calcite (ICCD 00-003-0612) are shown by XRD analysis, while peaks related to portlandite are not detected; however, μFT-IR confirms only the presence of vaterite and the lack of calcite; this discordance is probably due to the fact that μFT-IR analysis is a punctual technique, even though the analysis was performed on different points of the same sample. Finally, the results after three months confirm the presence of calcite only at 90% RH for both techniques.

The carbonation process of CaLoSil E50 at different RH conditions was also studied to compare its behavior with respect to calcium ethoxide. XRD results show that an RH value of 50% leads to the formation of the crystalline phase of aragonite (ICCD 00-001-0628) with typical reflections at $2\theta = 26°/45.7°$ (Figure 5a) [35]. The presence of aragonite is confirmed by μFT-IR, where the characteristic vibrational peak of aragonite at 855 cm^{-1} is shown (Figure 5b) [26,36]. The presence of aragonite could be due to some internal modification of vaterite [37].

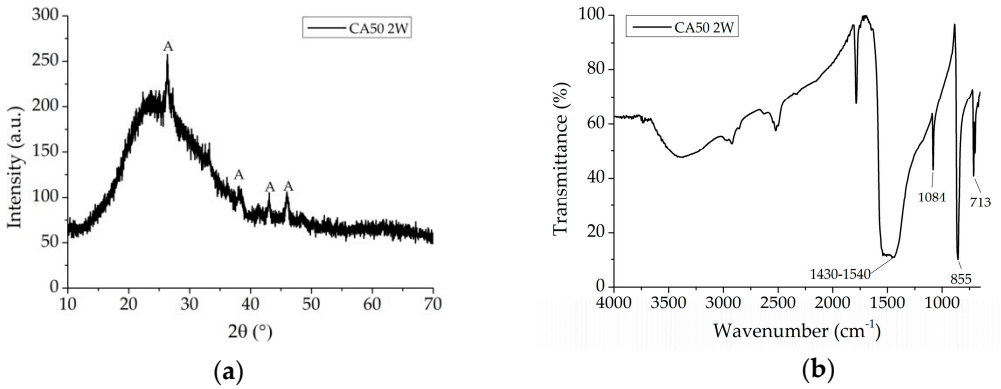

Figure 5. CaLoSilE50 at 50% RH after two weeks (CA50 2W): (**a**) XRD pattern; (**b**) μFT-IR spectrum. XRD peak assignments: A, aragonite

On the contrary, a higher quantity of water molecules at 90% RH leads to the formation of both vaterite (ICCD 00-001-1033) and calcite (ICCD: 01-072-1651) as shown by the XRD pattern in Figure 6a. These results are consistent with characteristic absorption peaks at 1085 and 745 cm^{-1} for vaterite and 713 cm^{-1} for calcite, shown by the μFT-IR spectrum (Figure 6b).

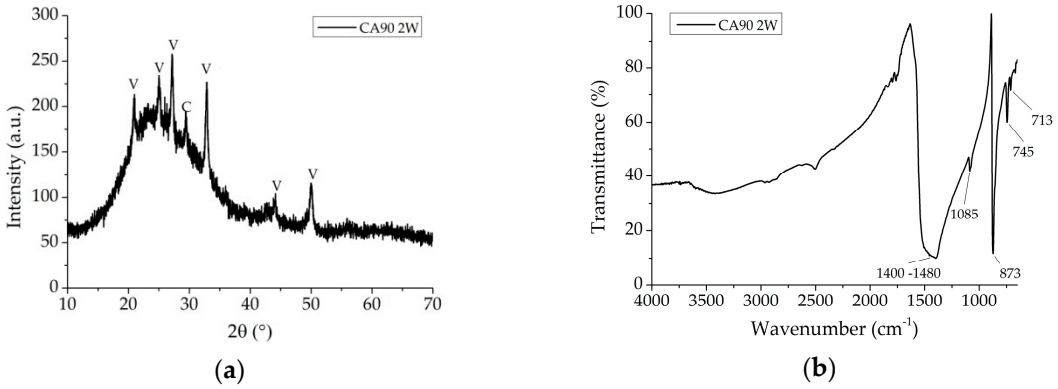

Figure 6. CaLoSilE50 at 90% RH after two weeks (CA90 2W): (**a**) XRD pattern; (**b**) μFT-IR spectrum. XRD peak assignments: C, calcite; V, vaterite.

After one month and three months, the XRD and μFT-IR results remain constant, confirming the presence of aragonite at 50% RH and vaterite and calcite at 90% RH.

Coating analysis highlights the complexity of the carbonation process, which always led to the formation of vaterite, the most kinetically favored, in all RH conditions, except for CA at 50% RH, for which aragonite is the formed phase [38]. It is interesting to underline how in the presence of a major quantity of water (higher RH condition) vaterite can partially transform to calcite, the most thermodynamically stable [38,39]. This evidence may be related to the process of dissolution of vaterite and subsequent recrystallization to calcite in the presence of water (90% RH).

3.3. Performance of Consolidation Treatments

All the stones samples submitted to an artificial ageing showed porosity changes: Noto stone from 30–34%, Vicenza stone from 31–28% and Lecce stone from 34–37%. In the case of Vicenza stone, the objective of the ageing was not achieved.

Table 1 presents the range of values between the minimum and the maximum quantities of the products retained for all lithotypes and application trials. The differences among the quantity of product retained for samples treated with the same product are influenced by the different shape of mock-ups (in accordance with the different analyses, mock-ups of different dimensions were necessary). More details of the product retained in relation to the different analyses for each type of stone are shown in Tables S1–S3 in the Supplementary Materials.

Table 1. Range of the amount of product retained after one month from the application.

Stone	Quantity of Product Retained (kg/m^2)			
	ET B1	ET B2	CA B1	CA B2
Noto	0.028–0.208	0.017–0.051	0.017–0.122	0.010–0.025
Vicenza	0.011–0.060	0.019–0.053	0.027–0.210	0.014–0.062
Lecce	0.016–0.115	0.019–0.114	0.012–0.097	0.010–0.022

The capillary water absorption coefficient (CWAC) was reduced after both application procedures and types of treatments for all considered lithotypes as showed by the % reduction in CWAC between treated and untreated samples, reported in Table 2. By comparing the two types of application procedures, it can be seen that for Vicenza stone and Noto stone, the decrease of CWAC due to ET is always higher with respect to CA.

Table 2. Water absorption coefficient, comparison before and after treatment. CWAC, capillary water absorption coefficient.

Stone	Reduction in CWAC %			
	ET B1	ET B2	CA B1	CA B2
Noto	28.8	23.1	15.8	15.9
Vicenza	36.9	30.2	29.3	25.5
Lecce	6.5	17.6	20.2	7.9

Regarding the water vapor permeability (Figure 7) all the treatments, except ET B1 applied on Lecce stone, led to a decrease of the g value, in accordance with the water absorption test for which ET B1 led to a small variation of CWAC for Lecce stone.

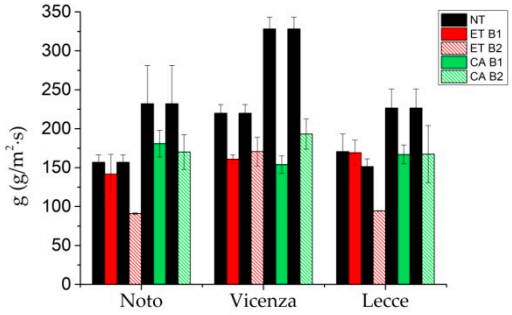

Figure 7. Water vapor permeability test results expressed as water vapor permeability coefficient (g) reported as a comparison before (NT = untreated) and after treatment.

Instead, Vicenza stone treated with CA, with both application procedures, shows a very high decrease. All treatments led to a reduction of the cumulative volume of pores for Lecce stone (except ET B2) and for Noto stone. Vicenza stone gives variable results, the largest one being obtained for ET B1, as can be concluded from the graphs in Figure 8.

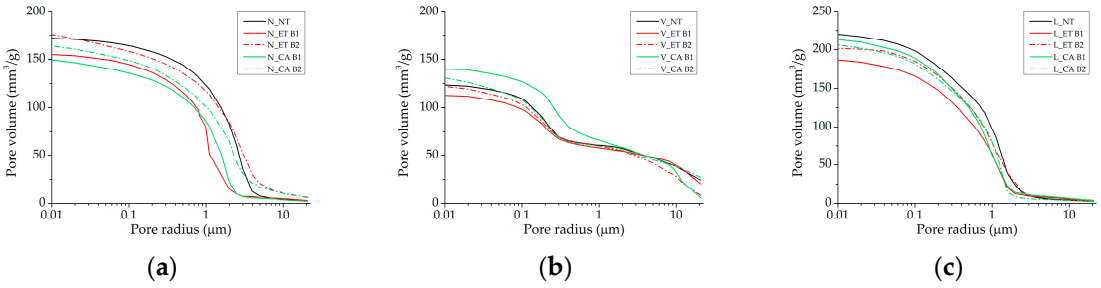

Figure 8. Pore volume (mm^3/g) versus pore radius reported as a comparison between untreated and treated samples: (**a**) Noto stone; (**b**) Vicenza stone; (**c**) Lecce stone.

Table 3 shows the colorimetric coordinate L^* before and after treatments and the relative color differences ΔE^* calculated using color Cie$L^*a^*b^*$ parameters acquired before and after treatment for application B1. ΔE^* variation referred to application B2 always lies under the threshold value ($\Delta E^* = 5$) [40,41] because the purpose of this application was to limit color variations to this value. For the application B1, only Vicenza stone shows ΔE^* parameters lower than five for both applied products; in fact, the coordinate L^* does not vary significantly before and after treatment. On the contrary, both ET and CA applied on Noto stone and Lecce stone lead to a whitening of the surface, as evident from the high variation of L^* values, and therefore, to a too high change of the surface color with a higher change for CA with respect to ET.

Table 3. Colorimetric coordinates L^* and relative color differences ΔE^* generated by consolidating products with both application procedures.

Stone	ET B1			CA B1		
	L^* Before	L^* After	ΔE^*	L^* Before	L^* After	ΔE^*
Noto	82.4	84.2	6.3 ± 0.2	83.6	86.9	9.3 ± 0.8
Vicenza	88.1	88.7	2.6 ± 0.2	88.1	88.3	2.3 ± 1.0
Lecce	80.9	82.8	6.9 ± 0.5	81.4	85.4	11.9 ± 0.1

SEM images were acquired to identify morphological variation of the surface due to the application of treatments. Despite the type of application procedure, a different behavior between ET and CA is always visible. Figure 9 presents SEM images acquired after the application procedure B1; while ET (Figure 9b,e,h) maintains a surface morphology similar to the untreated sample (Figure 9a,d,g); and CA forms a layer on the surface (Figure 9c,f,i).

Looking at the analyses overall, calcium ethoxide nanosuspension and CaLoSil E50 show different effects on the original properties of the limestones, especially in water transport properties. In fact, ET induces higher reduction of the capillary water absorption coefficient with both application procedures (except for Lecce ET B1). On the contrary, CA causes a higher reduction of water vapor permeability, possibly due to the formation of a dense layer on the treated surface after the application B1 as shown by the SEM images. Both treatments applied with application protocol B1 show a low aesthetic compatibility with a ΔE^* variation higher than five for Lecce stone and Noto stone, with worse results for CA. Instead, for Vicenza stone, the chromatic variations range within acceptable limits.

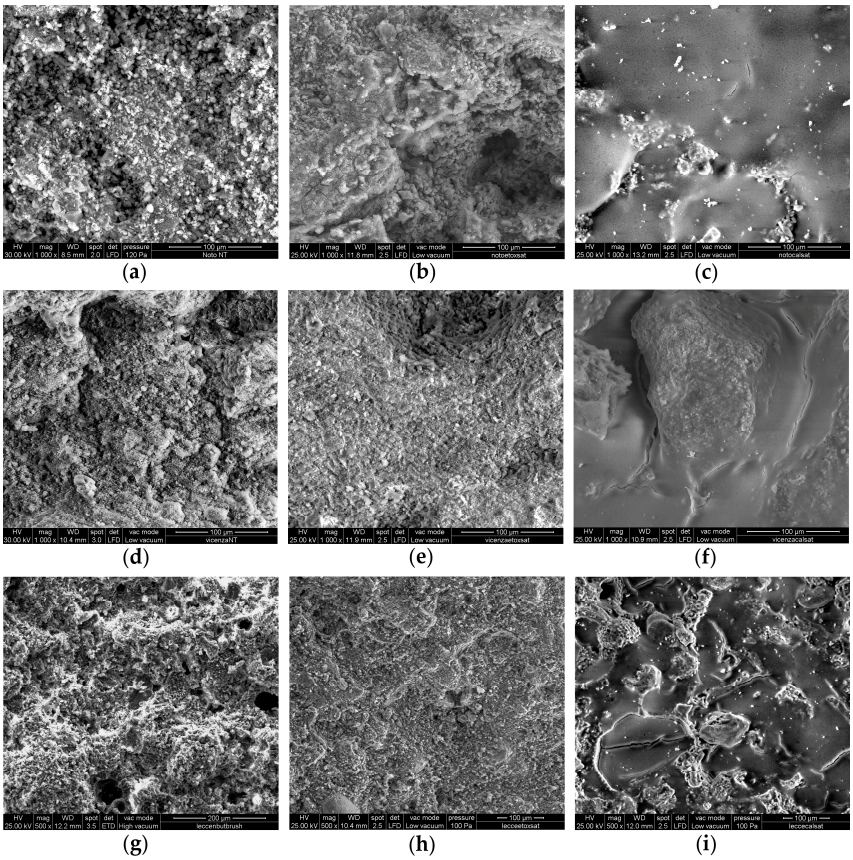

Figure 9. SEM images of samples treated with protocol B1: (**a**) Noto untreated; (**b**) Noto ET; (**c**) Noto CA; (**d**) Vicenza untreated; (**e**) Vicenza ET; (**f**) Vicenza CA; (**g**) Lecce untreated; (**h**) Lecce ET; (**i**) Lecce CA.

To understand the penetration depth reached by the treatments applied by brush till saturation (B1), UPV and DRMS were used. Differently from Noto stone and Lecce stone for which no good penetration is detected with both techniques, UPV on Vicenza stone treated with ET (Figure 10a) shows a small variation of stone density, connected to a consolidation effect, in the first 5–10 mm from the treated surface. However, these UPV results are not confirmed by the hardness profile obtained by the three holes of DRMS (Figure 10b); the heterogeneity of the Vicenza stone and the weak consolidation effect may explain the obtained results. However, after treatment, higher peaks were registered in the first 10 mm of the individual profiles. Further research using other methods and data analysis particularly relevant for heterogeneous materials, combined with weak consolidation effects, will clarify this effect [42,43].

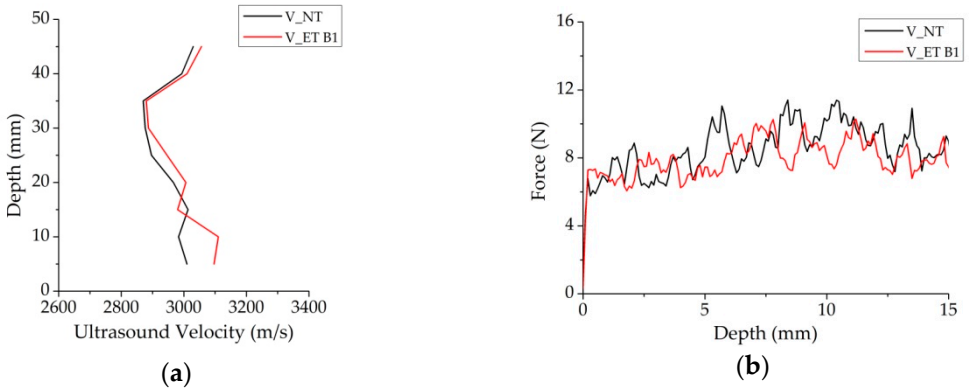

Figure 10. (**a**) Ultrasonic and (**b**) drilling profiles of Vicenza stone treated with ET B1reported as a comparison before and after treatment.

4. Conclusions

In this study, an investigation of a new conservation product, calcium ethoxide, specific for limestones, was carried out, and its efficiency and compatibility as a consolidating agent were compared with a reference treatment, CaLoSil E50.

The characterization of the kinetic and the reaction pathway of the carbonation process of calcium ethoxide showed that it is a quick process: peaks related to the formation of calcium carbonate were registered after two minutes from the beginning of the reaction, while the process ends after six hours. Concerning the reaction pathway, both possible mechanisms are followed: (i) insertion of a CO_2 molecule within the Ca–O bond followed by hydrolysis and alcohol elimination; and (ii) the hydrolysis reaction of the ethoxide with the formation of calcium hydroxide as an intermediate, which subsequently carbonates. The kinetic and the reaction pathway of calcium ethoxide are not influenced by the presence of powdered limestone. The combined approach of XRD and μFT-IR is a valid tool to study these processes.

Coating analyses highlight that higher relative humidity favors the formation of calcite both for $Ca(OEt)_2$ and for CaLoSil E50, in accordance with reference data reported for nanolimes.

Regarding the application of calcium ethoxide on limestones, the most interesting results are obtained by applying calcium ethoxide on Vicenza stone with the application by brush till saturation (ET B1), as seen from the combination among modifications of water transport properties, the consolidation effect and colorimetric variation. Differently from calcium ethoxide, the reference product causes a small reduction of water absorption by capillarity and a greater reduction of water vapor permeability, an effect probably due to the formation of a dense layer on the treated surface. Furthermore, it causes a higher surface color variation with respect to calcium ethoxide.

Studies are currently under way to integrate the results of previous research involving the study of the carbonation process of calcium ethoxide once applied on limestones. Analyses will be performed

to evaluate the persistence of phases different from calcite and on the acquisition of information about the penetration depth reached by the treatment applied with a pre-set number of brush strokes.

Supplementary Materials: The following are available online at www.mdpi.com/2079-6412/8/3/103/s1: Table S1: Amount of product retained according to different types of analysis for Noto stone; Table S2: Amount of product retained according to different types of analysis for Vicenza stone; Table S3: Amount of product retained according to different types of analysis for Lecce stone.

Acknowledgments: The NANOMATCH Project (Nano-systems for the conservation of immoveable and moveable polymaterial cultural heritage in a changing environment) has received funding from the European Union's Seventh Program for research, technological development and demonstration under Grant Agreement No. [283182]. Naida El Habra, from CNR-ICMATE, Istituto di Chimica della Materia Condensata e di Tecnologie per l'Energia, Padova, is kindly acknowledged for performing XRD measurements.

Conflicts of Interest: The authors declare no conflict of interest.

References

1. Brimblecombe, P. History of air pollution and damage to the cultural heritage of European cities. In *Science, Technology and European Cultural Heritage*; Baer, N.S., Sabbioni, C., Sors, A.I., Eds.; Butterworth-Heinemann: Oxford, UK, 1991; pp. 51–66.
2. Maravelaki, P.; Bertoncello, R.; Biscontin, G.; Battaglin, G.; Zendri, E.; Tondello, E. Investigation of the surface processes on exposed limestones. In *Symposium J–Materials Issues in Art and Archaeology III*; Vandiver, P.B., Ed.; Materials Research Society: Pittsburgh, PA, USA, 1992; Volume 267, p. 943. [CrossRef]
3. Martínez-Martínez, J.; Benavente, D.; Gomez-Heras, M.; Marco-Castaño, L.; García-Del-Cura, M.Á. Non-linear decay of building stones during freeze-thaw weathering processes. *Constr. Build. Mater.* **2013**, *38*, 443–454. [CrossRef]
4. Cardell, C.; Delalieux, F.; Roumpopoulos, K.; Moropoulou, A.; Auger, F.; Van Grieken, R. Salt-induced decay in calcareous stone monuments and buildings in a marine environment in SW France. *Constr. Build. Mater.* **2003**, *17*, 165–179. [CrossRef]
5. Warscheid, T.; Braams, J. Biodeterioration of stone: A review. *Int. Biodeterior. Biodegrad.* **2000**, *46*, 343–368. [CrossRef]
6. Favaro, M.; Tomasin, P.; Ossola, F.; Vigato, P.A. A novel approach to consolidation of historical limestone: The calcium alkoxides. *Appl. Organomet. Chem.* **2008**, *22*, 698–704. [CrossRef]
7. Ossola, F.; Tomasin, P.; De Zorzi, C.; El Habra, N.; Chiurato, M.; Favaro, M. New Calcium Alkoxides for Consolidation of Carbonate Rocks. Influence of Precursors' characteristics on morphology, crystalline phase and consolidation effects. *New J. Chem.* **2012**, *36*, 2618–2624. [CrossRef]
8. Duchêne, S.; Detalle, V.; Favaro, M.; Ossola, R.; Tomasin, P.; De Zorzi, C.; El Habra, N. Nanomaterials for the consolidation of marble and wall paintings. In Proceedings of the 12th International Congress on the Deterioration and Conservation of Stone Columbia University, New York, NY, USA, 21–25 October 2012; pp. 1–9.
9. Bourguignon, E.; Tomasin, P.; Detalle, V.; Vallet, J.; Labouré, M.; Olteanu, I.; Chiurato, M.A.; Bernardi, A.; Becherini, F. Calcium alkoxides as alternative consolidants for wall paintings: Evaluation of their performance in laboratory and on site, on model and original samples, in comparison to conventional products. *J. Cult. Herit.* **2017**, *29*, 54–66. [CrossRef]
10. Natali, I.; Tomasin, P.; Becherini, F.; Bernardi, A.; Ciantelli, C.; Favaro, M.; Favoni, O.; Pérez, V.J.F.; Olteanu, I.D.; Dolores, M.; et al. Innovative consolidating products for stone materials: Field exposure tests as a valid approach for assessing durability. *Herit. Sci.* **2015**, *3*, 1–13. [CrossRef]
11. Favaro, M.; Chiurato, M.; Tomasin, P.; Ossola, F.; Habra, E.; Svensson, I.; Beckers, E.; Bernardi, A. Calcium and magnesium alkoxides for conservation treatment of stone and wood in built heritage. In Proceedings of the Built Heritage 2013: Monitoring Conservation Management, Milan, Italy, 18–20 November 2013; pp. 1296–1303.
12. Favaro, M.; Chiurato, M.; Tomasin, P.; Ossola, F.; Habra, E.; Brianese, N.; Svensson, I.; Beckers, E.; Perez, V.J.F.; Romero Sánchez, M.D.; et al. Alkaline earth alkoxides for conservation treatment of stone and wood in built heritage. In Proceedings of the 3rd European Workshop on Cultural Heritage Preservation, EWCHP 2013, Bozen, Italy, 15–17 September 2013; pp. 105–111.

13. *Final Report Summary—NANOMATCH (Nano-Systems for the Conservation of Immoveable and Moveable Polymaterial Cultural Heritage in a Changing Environment)*; Consiglio Nazionale delle Ricerche: Rome, Italy, 2015; Available online: https://cordis.europa.eu/result/rcn/163221_en.html (accessed on 12 March 2018).
14. CaLoSiL®. Colloidal nano-particles of lime for stone and plaster consolidation. Technical Leaflet. IBZ-Salzchemie GmbH & Co. KG.: Halsbrücke, Germany. Available online: https://ibz-freiberg.de/downloads/pdf/produkte/tm/eng/CaLoSiL_E_IP_NP.pdf (accessed on 12 March 2018).
15. Greenspan, L. Humidity fixed points of binary saturated aqueous solutions. *J. Res. Natl. Bur. Stand. Sect. A Phys. Chem.* **1977**, *81*, 89. [CrossRef]
16. Gordillo, J.R.; Pérez, M.P.S. Comportamiento físico del mármol blanco de Macael (España) por oscilación térmica de bajo y medio rango Performance of Spanish white Macael marble exposed to narrow- and medium-range temperature cycling. *Mater. Constr.* **2010**, *60*, 127–141. [CrossRef]
17. *NORMAL 4/80 Distribuzione del Volume dei Pori in Funzione del Loro Diametro (Italian Normative on Stone Material—Distribution of Pores Volume vs Their Diameter)*; Commissione Beni Culturali UNI NORMAL: Rome, Italy, 1980.
18. *UNI EN 10859:2000 Beni Culturali Materiali Lapidei Naturali ed Artificiali: Determinazione Dell'assorbimento D'acqua per Capillarità*; Commissione Beni Culturali UNI NORMAL: Rome, Italy, 2010.
19. *DIN 52615 Testing of Thermal Insulating Material; Determination of Water Vapour Permeability of Construction and Insulating Materials*; Deutsches Institut fur Normung E.V. (DIN): Berlin, Germany, 1987.
20. *NORMAL 43/93 Misure Colorimetriche di Superfici Opache (Italian Normative on Stone Material—Colorimetric Measurement of Opaque Surfaces)*; Commissione Beni Culturali UNI NORMAL: Rome, Italy, 1994.
21. Adler, H.H.; Kerr, P.F. Infrared absorption frequency trends for anhydrous normal carbonates. *Am. Mineral.* **1963**, *48*, 124–137.
22. Hazen, R.M.; Downs, R.T.; Jones, A.P.; Kah, L. Carbon Mineralogy and Crystal Chemistry. *Rev. Mineral. Geochem.* **2013**, *75*, 7–46. [CrossRef]
23. Essabir, H.; Bensalah, M.O.; Rodrigue, D.; Bouhfid, R.; Qaiss, A.E.K. A comparison between bio and mineral calcium carbonate on the properties of polypropylene composites. *Constr. Build. Mater.* **2017**, *134*, 549–555. [CrossRef]
24. Wei, H.; Shen, Q.; Zhao, Y.; Wang, D.; Xu, D. Influence of polyvinylpyrrolidone on the precipitation of calcium carbonate and on the transformation of vaterite to calcite. *J. Cryst. Growth* **2003**, *250*, 516–524. [CrossRef]
25. Meiron, O.E.; Bar-David, E.; Aflalo, E.D.; Shechter, A.; Stepensky, D.; Berman, A.; Sagi, A. Solubility and Bioavailability of Stabilized Amorphous Calcium Carbonate. *J. Bone Miner. Res.* **2011**, *26*, 364–372. [CrossRef] [PubMed]
26. Andersen, F.A.; Brečević, L. Infrared Spectra of Amorphous and Crystalline Calcium Carbonate. *Acta Chem. Scand.* **1991**, *45*, 1018–1024. [CrossRef]
27. Rodriguez-Blanco, J.D.; Shaw, S.; Benning, L.G. The kinetics and mechanisms of amorphous calcium carbonate (ACC) crystallization to calcite, via vaterite. *Nanoscale* **2011**, *3*, 265–271. [CrossRef] [PubMed]
28. Rodriguez-Navarro, C.; Suzuki, A.; Ruiz-Agudo, E. Alcohol Dispersions of Calcium Hydroxide Nanoparticles for Stone Conservation. *Langmuir* **2013**, *29*, 11457–11470. [CrossRef] [PubMed]
29. Cumaran Arunasalam, V.; Baxter, I.; Darr, J.A.; Drake, S.R.; Hursthouse, M.B.; Abdul Malik, K.M.; Mingos, D.M.P. Insertion reactions of small molecules into group 2 metal alkoxides; structural characterization of $[Mg_9(\mu_5\text{-}CO_3)(O_2COMe)_8(\mu_3\text{-}OMe)_8(MeOH)_{13}]\cdot MeOH\cdot C_7H_8$. *Polyhedron* **1998**, *17*, 641–657. [CrossRef]
30. Zhao, Z.; Xia, Y.; Xue, J.; Wu, Q. Role of *E. coli*—Secretion and Melamine in Selective Formation of $CaC_2O_4\cdot H_2O$ and $CaC_2O_4\cdot 2H_2O$ Crystals. *Cryst. Growth Des.* **2014**, *14*, 450–458. [CrossRef]
31. Zhang, X.; Glasser, F.P.; Scrivener, K.L. Reaction kinetics of dolomite and portlandite. *Cem. Concr. Res.* **2014**, *66*, 11–18. [CrossRef]
32. Chang, J.; Li, Y.; Cao, M.; Fang, Y. Influence of magnesium hydroxide content and fineness on the carbonation of calcium hydroxide. *Constr. Build. Mater.* **2014**, *55*, 82–88. [CrossRef]
33. Chen, J.; Xiang, L. Controllable synthesis of calcium carbonate polymorphs at different temperatures. *Powder Technol.* **2010**, *189*, 64–69. [CrossRef]
34. Nan, Z.; Chen, X.; Yang, Q.; Wang, X.; Shi, Z.; Hou, W. Structure transition from aragonite to vaterite and calcite by the assistance of SDBS. *J. Colloid Interface Sci.* **2008**, *325*, 331–336. [CrossRef] [PubMed]

35. Kontoyannis, C.G.; Vagenas, N.V. Calcium carbonate phase analysis using XRD and FT-Raman spectroscopy. *R. Soc. Chem.* **2000**, *125*, 251–255. [CrossRef]
36. Gopi, S.; Subramanian, V.K.; Palanisamy, K. Aragonite—calcite—vaterite: A temperature influenced sequential polymorphic transformation of $CaCO_3$ in the presence of DTPA. *Mater. Res. Bull.* **2013**, *48*, 1906–1912. [CrossRef]
37. Gabrielli, C.; Jaouhari, R.; Joiret, S.; Maurin, G. In situ Raman spectroscopy applied to electrochemical scaling. Determination of the structure of vaterite. *J. Raman Spectrosc.* **2000**, *31*, 497–501. [CrossRef]
38. López-Arce, P.; Gómez-Villalba, L.S.; Martínez-Ramírez, S.; Alvarez de Buergo, M.; Fort, R. Influence of relative humidity on the carbonation of calcium hydroxide nanoparticles and the formation of calcium carbonate polymorphs. *Powder Technol.* **2011**, *205*, 263–269. [CrossRef]
39. Gomez-Villalba, L.S.; López-Arce, P.; De Buergo, M.A.; Fort, R. Structural stability of a colloidal solution of $Ca(OH)_2$ nanocrystals exposed to high relative humidity conditions. *Appl. Phys. A Mater. Sci. Process.* **2011**, *104*, 1249–1254. [CrossRef]
40. Delgado Rodrigues, J.; Grossi, A. Indicators and ratings for the compatibility assessment of conservation actions. *J. Cult. Herit.* **2007**, *8*, 32–43. [CrossRef]
41. Sasse, H.S.; Snethlage, R. Methods for the evaluation of stone conservation treatments. In *Saving Our Architectural Heritage. The Conservation of Historic Stone Structures: Report of Dahlem Workshop on Saving our Architectural Heritage, Berlin, Germany, March 3–8, 1996*; Baer, N.S., Snethlage, R., Eds.; John Wiley & Sons: New York, NY, USA, 1997; p. 225.
42. Mimoso, J.; Costa, D. The DRMS drilling technique with pilot holes. In Proceedings of the Heritage Weather. Conservation Conference HWC-2006, Madrid, Spain, 21–24 June 2006; Volume 2, pp. 651–655.
43. Delgado Rodrigues, J.; Costa, D. A new interpretation methodology for microdrilling data from soft mortars. *J. Cult. Herit.* **2016**, *22*, 951–955. [CrossRef]